

DEVELOPMENT AND TESTING OF AN ADDITIVELY MANUFACTURED LATTICE FOR DEMO LIMITERS

N. MANTEL¹, D. BOWDEN¹, S.S. HERASHCHENKO³, M. FURSDON¹, A. D. L. HANCOCK¹, I.E. GARKUSHA³, J. ROBERTS¹, M. SHABANI¹, V.A. MAKHLAI³, A. VON MÜLLER², T. R. BARRETT¹, J.-H. YOU²

¹ United Kingdom Atomic Energy Authority Culham Science Centre, Abingdon, UK

² Max Planck Institute for Plasma Physics, Garching, Germany

³ NSC KIPT, National Science Center, 'Kharkov Institute of Physics and Technology', Institute of Plasma Physics, Kharkiv., Ukraine

E-mail: xxx@xxx.xx

Received xxxxxx

Accepted for publication xxxxxx

Published xxxxxx

Abstract

In the conceptual design of EU-DEMO, damage to plasma-facing components under disruption events is planned to be mitigated by specific sacrificial limiter components. A new limiter concept has been proposed using lattice structures fabricated with tungsten powder by additive manufacturing techniques. The major potential benefits of using a lattice structure for limiters are the possibility to customise the thermal conductivity and structural compliance of these components to manage temperatures and stress within material limits and lower the sensitivity to crack propagation. This paper presents the results of the first investigations into the production, characterisation, and high heat flux testing of these lattices to assess their suitability for DEMO limiters. First stage prototypes have been manufactured from tungsten and tungsten tantalum mixed powder with two distinct laser powder bed fusion processes, namely pulsed laser and continuous laser with heated bed. The samples are characterised in terms of mass, volume, density, extent of microcracks and voids, level of un-melted or partially melted particulates, texture and grain size, as well as tantalum segregation when applicable. High transient (0.25ms) heat load testing, with hydrogen plasma of energy density up to $\sim 3 \text{ MJ}\cdot\text{m}^{-2}$ was carried out at KIPT on the QSPA Kh-50. These tests have shown that the energy absorbed by latticed targets preheated at 500°C is close to that absorbed by solid tungsten, suggesting that they may be used for limiter applications with the added advantage of adjustment of the heat transfer and stiffness performance by geometry design or material properties.

Keywords: Additive manufacturing, AM, High heat flux testing, HHF, Tungsten, Tantalum, WTa

1. INTRODUCTION

In the conceptual design of EU-DEMO, damage to plasma-facing components as a result of disruption events leading to plasma-wall contact is a major concern [1]. This is planned to

be mitigated by specific sacrificial limiter components. A new limiter concept has been proposed using lattice structures fabricated with tungsten powder by additive manufacturing (AM) techniques. The major potential benefits of using a lattice structure for limiters are the possibility to customise the thermal conductivity and structural compliance of the

structure to manage temperatures and stress within material limits and lower the sensitivity to crack propagation. Geometries optimised for thermal behaviour were defined by parametric study in [2].

Numerical analysis results [2] for a theoretical component show that whilst W lattices may bring decisive structural benefits, there are significant manufacturing challenges that need to be overcome to reliably produce a component based on this concept, and testing is the key to validate the potential and limits of the technology, exposed by analysis.

This paper presents the results of the first investigations into the production, characterisation, Plasma Surface Interaction (PSI) and mass loss from the high heat flux testing plasma, of the lattices to assess their suitability for EU-DEMO limiters.

2. METHODS

2.1. PRODUCTION

In this project, the processing of pure tungsten (W) and a tungsten-6wt.% tantalum (W-6%Ta) alloy by Laser Powder Bed (LPB) AM was investigated. W-6%Ta was chosen for its enhanced ductility compared to pure W. This was in order to reduce crack initiation and propagation as well as to improve processability [3]. The main goal is to achieve high dimensional accuracy and density of three geometries of built lattice structures L2 ($A=1.6$, $L=0.334\text{mm}$, $r=0.15\text{mm}$, $k=0.167$), L3 ($A=1.6$, $L=0.556\text{mm}$, $r=0.25\text{mm}$, $k=0.278$), L6 ($A=0.5$, $L=0.556\text{mm}$, $r=0.25\text{mm}$, $k=0.278$), where A is the aspect ratio, L is ligament length, r the ligament radius, k the upscaling factor as defined in [2]. To achieve this goal, two distinct production routes were pursued:

- W-6%Ta at the company Renishaw using a pulsed laser, and a mix of W and Ta powder for crack suppression purposes [3].

- W at Fraunhofer Institute for Casting, Composite and Processing Technology IGCV using a continuous laser following the optimisation process from [4].

Before production of the final W-6%Ta lattice cube structures, optimization of the process of producing laser powder bed fusion (LPBF) tungsten tantalum was carried out on solid (non-lattice) cube components. This was achieved from five builds of six sample cubes per build plate.

The primary process parameters varied were the hatch distance (the spacing between neighbouring scan vectors), the laser point diameter, exposure time and energy density. The optimisation was achieved by a method of stepping each process parameter in small steps as per TABLE 1 and observing trends in density and microstructure on simple cube geometry. A density of 98.7% was observed for the selected parameter (Laser power 350W, Hatch distance 70 μm , point distance 30 μm , Exposure time 100 μs , Energy density $\text{J}\cdot\text{mm}^{-2}$).

With each build, the cubes were sectioned and scanned by SEM (see e.g. FIG 1) to observe defects and assess density.

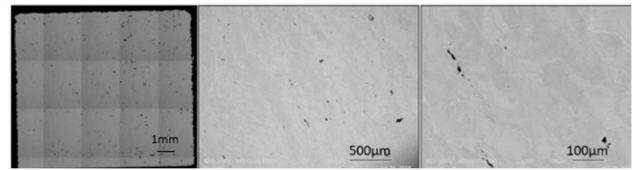


FIG 1: Cross-section of optimization W-6%Ta sample using the selected build parameters. From left to right optical, SEM Back Scattered Electron (BSE) x50 MAG and x200 MAG.

TABLE 1: PROCESS PARAMETERS WITH SELECTED PARAMETERS IN BOLD

Process parameter	Tested value
Laser Power (W)	300 \ 320 \ 350 \ 400
Hatch distance (μm)	50 \ 70 \ 100
Point distance (μm)	30 \ 45 \ 50 \ 60 \ 70
Exposure time (μs)	100 \ 115 \ 150 \ 200
Energy density ($\text{J}\cdot\text{mm}^{-2}$)	12.00 \ 13.33 \ 14.00 \ 16.67 \ 19.20 \ 20.00

2.2. CHARACTERISATION

2.2.1. Imaging

The AM W and W-6%Ta specimens were prepared to scanning electron microscopy (SEM) electron backscatter diffraction (EBSD) quality, using standard preparation procedures to a 1 μm diamond finish. Polishing using 0.04 μm -diameter colloidal silica was then conducted for 40 minutes, with a rinse of the polishing cloth every 5-minutes to remove particulate debris. A final cleaning step utilising ultrasonic agitation was carried out.

Imaging of the top face (normal to build direction) of all AM W and W-6%Ta samples was carried out using a Zeiss EVO-10 SEM, using secondary electron (SE) imaging at an accelerating voltage of 20 kV and 100 pA probe current.

2.2.2. Lattice conformity and build quality

The use of the software package Fiji-ImageJ v1.51u enabled the comparison of the lattice geometry specified within the computer aided design (CAD) geometry, to the AM lattice structures imaged in the SEM. CAD images in the build plane were matched to the same physical position at the surface of the AM cube. SEM-SE micrographs taken at the surface of the AM cube were processed using image thresholding such that only the pores (spaces in lattice structure) were visible. A particle size analysis routine was conducted on these pores, and the process was repeated for the CAD geometry. From the particle size measurement routine, the length and width of these features was determined using Ferets diameter measurement, which enables the measurement of irregular shapes (such as pores) along a specified direction. This was used to measure the principal directions of an oval (length and width), which best represented the lattice pore

features. By setting a threshold value in the greyscale SEM images obtained for the AM samples, it was possible to compare the deviation in the length and width measurements from the AM samples, to the measurements obtained from the CAD geometry, a percentage deviation of actual AM geometry versus the intended geometry could be obtained.

The area conformity is obtained through a similar approach, except that after thresholding the image, the number of pixels residing in the lattice pore regions in the SEM sample and CAD model is compared. The images are equally scaled, and the SEM measurement is divided by the CAD model measurement to produce a percentage area conformity measurement.

In all measurements reported here, a geometric conformance value below 100% indicates overbuild of the AM structure when compared to the original CAD geometry.

2.2.3. Thermal diffusivity measurement

The thermal diffusivity of the AM W-6%Ta material was assessed using a Netzsch laser flash analyser (LFA). In these tests the material produced did not feature a lattice, but instead was comprised of a fully-filled AM sample. Cylindrical samples of dimensions 12.5 mm \varnothing \times 3 mm-thick were produced by Renishaw using the optimal build settings indicated in TABLE 1. LFA measurements were taken initially at room temperature, followed by 100°C increments to a maximum temperature of 1500°C. An Ar purge was used throughout testing. A 500V laser was applied to the sample in 0.6 ms pulse durations, with each pulse approximately 90 seconds apart for a total of five pulses at each temperature step.

2.3. HIGH-HEAT FLUX TESTING

To replicate the high heat load potentially applied to the limiter, a campaign of High Heat Flux (HHF) tests subjected L6 type lattice (only type available at the time of the preliminary test), AM W and AM W-6%Ta to “extreme” fast transient heat loads to compare with the ‘established baseline’ cold rolled W (CRW) armour material.

2.3.1. Sample and experimental conditions

8 solid non-polished CRW samples, from an DEMO monoblock prototype part, were supplied to act as base line material and for comparison to the results from experiment [5]. 12 L6 AM W-6%Ta non-polished lattices, 12 L6 AM W-6%Ta polished and 4 L6 AM W polished lattice samples were also tested. The aim of the polishing was to improve the microscopic observation, and reduce the number of loosely attached particles at the surface of the sample leading to overestimation of the mass loss. Typical sample preparation steps were followed using diamond polishing to produce a 1 μ m surface finish. This was followed by vibration polishing using colloidal silica for 3h. Approximately 100-120 μ m of

the surface layer was removed in each case. A general view of samples is presented in FIG 2.

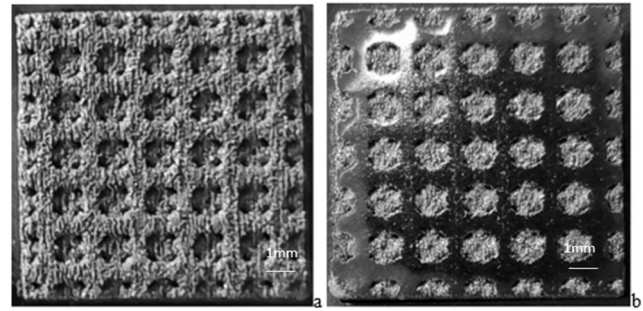


FIG 2: General views of non-polished (a) and polished (b) AM W-6%Ta latticed samples.

HHF testing of samples has been performed within the Quasi-Stationary Plasma Accelerator (QSPA) Kh-50 at the Kharkov Institute of Physics and Technology (KIPT) [5]. CRW, AM lattice W and W-6%Ta samples were exposed for both cross-comparison and comparison with existing data.

Groups of four targets were exposed simultaneously to one chosen load. The base temperature of the samples was 500°C. A tungsten diaphragm was used to protect the holder during the tests, as shown in FIG 3.

The energy density absorbed by the target (q) as well as energy density of the impacting plasma stream (Q) were measured with thermocouple calorimeters. Q was measured by a single calorimeter without the samples. Then, the calorimeter was inserted in the central hole on the rear of the sample. Thus, it became possible to measure the energy density (q) delivered to the surface [5]. Observations of plasma interactions with exposed surfaces and droplets monitoring were performed with the high-speed PCO AG complementary metal-oxide-semiconductor (CMOS) camera.

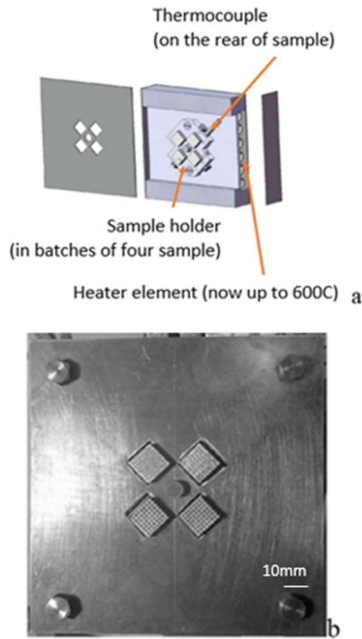


FIG 3: Holder scheme used for HHF testing using QSPA at KIPT. a) Schematic view of samples in the holder, b) image taken showing lattice samples in the final test assembly.

Experimental conditions around the expected evaporation threshold reported in [5] were set as follows: targets were exposed for 0.25 ms to incoming plasma stream energy density of $1.8 \text{ MJ}\cdot\text{m}^{-2}$ (5 plasma pulses), $2.3 \text{ MJ}\cdot\text{m}^{-2}$ (5 plasma pulses), and $\leq 3 \text{ MJ}\cdot\text{m}^{-2}$ (5 plasma pulses). Images of the sample were taken 1.2 ms after the start of the plasma with a time frame of 1.2 ms.

Mass measurements were performed before the first and after the last pulse to monitor the mass loss (ΔM) after the pulse to an accuracy of: $\pm 15 \mu\text{g}$.

3. RESULTS AND DISCUSSION

3.1. PRODUCTION AND CHARACTERISATION

3.1.1. Build quality and conformity

It is shown in TABLE 2, that out of the AM W-6%Ta lattices geometry (L2, L3, L6) produced by the company Renishaw, that the L3 lattice has the best conformity to the intended CAD geometry. The results of this table were ascertained by taking Feret length and width measurements of the intended CAD features, and comparing these to the as-built features, as shown in FIG 4. The overbuild in all lattice types is witnessed from the left handside of the images (red shading indicates the intended surface build geometry from CAD model). It is important to note that the L3 lattice contains the coarsest lattice features, which would enable superior conformity in the final built product. Interestingly, the Fraunhofer lattices had overall superior geometric conformity when compared to the Renishaw samples (TABLE 2). The

cause of this may be the use of a continuous laser at Fraunhofer, versus a pulsed laser used at Renishaw which may lead to issues of unreliable and inaccurate powder consolidation.

TABLE 2: SUMMARY OF W6%Ta & W LATTICE CONFORMITY FOR L2, L3 AND L6 GEOMETRY

Material	AM build laser type	Lattice ID	Area conformity (%)	Feret length conformity (%)	Feret width conformity (%)
AM W6%Ta	Pulsed	L2	42	79	68
		L3	82	89	96
		L6	55	72	63
AM W	Continuous	L2	99	91	97
		L3	88	93	87
		L6	94	99	97

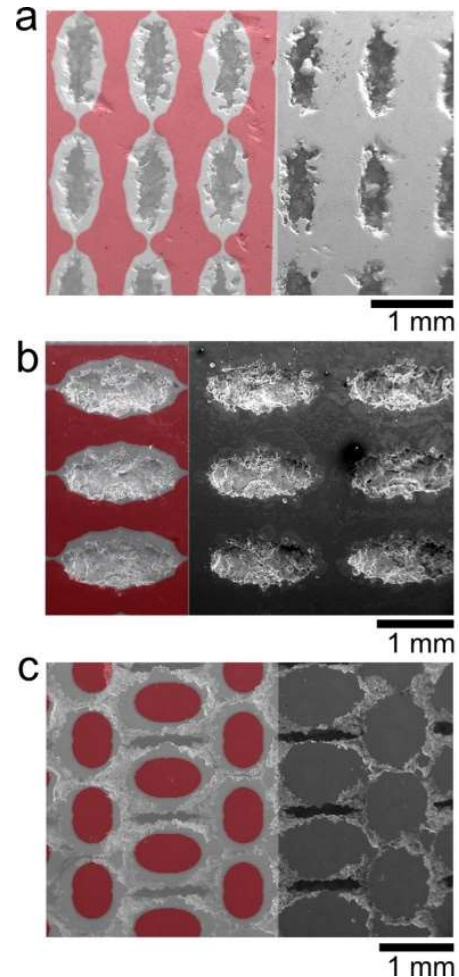


FIG 4: Comparison of the intended CAD geometry against SEM-SE micrographs of the produced Renishaw W-6%Ta AM lattices of types: a) L2, b) L3 and c) L6. The CAD geometry is shaded red

to indicate the in-plane solid surface. Overbuilding of the solid surface is observed in all cases.

3.1.2. Thermal diffusivity

The thermal diffusivity of the non-lattice version of the AM W-6%Ta was conducted using LFA. It was observed that the diffusivity decreased from its value of $26.435 \text{ mm}^2\cdot\text{s}^{-1}$ at $\sim 25^\circ\text{C}$, to $22.456 \text{ mm}^2\cdot\text{s}^{-1}$ at $\sim 1500^\circ\text{C}$ (FIG 5). When compared to pure W [6], the thermal diffusivity of AM W-6%Ta is reduced by 63% at $\sim 25^\circ\text{C}$. At 1500°C , this is less pronounced at a 47% reduction. Interestingly, unlike pure W, the AM W-6%Ta thermal diffusivity remains relatively stable throughout the temperature range ($25 - 1500^\circ\text{C}$), reducing by only 15% at 1500°C compared to a 40% reduction in pure W (at $\sim 1100^\circ\text{C}$). The overall reduction in thermal diffusivity of W-6%Ta is comparable to that of W-Re [7]. Re has been found to cause a reduction in thermal diffusivity when alloyed with W [7]. In this same way, Ta appears to have a similar effect of suppressing the thermal diffusivity when alloyed with W. It is interesting to note, that the 6 wt.% Ta addition appears to reduce the thermal diffusivity of the AM W-6%Ta to a comparable level as witnessed in pure Ta [8] (FIG 5). This does indicate potential favourability for a W-6%Ta limiter to act as a good thermal insulator, protecting sensitive materials beneath the plasma-facing layer, and ensuring that any melting would be localised at the limiter surface. But in a scenario requiring efficient thermal conduction to cooling components, the W-6%Ta would not perform as favourably as conventional W.

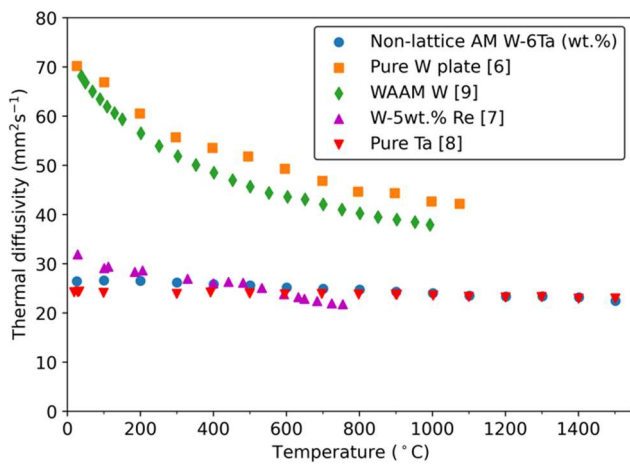


FIG 5: Thermal diffusivity measurement of AM W-6%Ta in non-lattice form, compared to pure W plate [6], WAAM W [9], W-5Re (wt.%) [7] and pure Ta [8]. The thermal diffusivity of AM W-6Ta is observed to follow a similar trend to that of pure Ta across the entire temperature range tested ($25 - 1500^\circ\text{C}$).

A comparison between the thermal diffusivity of pure W and wire-arc additive manufactured (WAAM) W [9] was carried out to understand whether the reduction in thermal diffusivity observed in the AM W-6%Ta was a result of the

AM process. The comparison between the two material forms is shown in FIG 5. In this case, good agreement in thermal diffusivity can be observed, with the small reduction in the case of the WAAM W, likely due to the reduced densification of the AM material. Unfortunately, a direct comparison with LPB W could not be located in the literature but based on the comparison to WAAM it is believed that the use of AM alone, does not introduce a significant reduction in thermal diffusivity. It is therefore believed that the substantial reduction in thermal diffusivity observed in W-6%Ta may be a result of the alloy chemistry and addition of 6 wt.% Ta. However, it is noted that microstructural features such as texture, porosity and grain morphology may influence the thermal properties in such materials, as has been observed in studies of alternate materials [10].

3.2. HIGH-HEAT FLUX TESTING

3.2.1. Energy density delivered/absorbed

The results of measurements by thermocouple of the energy density absorbed by latticed surfaces (q) were compared with those of CRW surfaces, as measured previously in [5] and during the tests for equivalent impacting plasma energy density (Q). Although variations were observed, it can be concluded that they were within the measurement error i.e. insignificant (FIG 6). Data on the graph corresponds to the mean value with a confidence interval of 80%, measured over 5 plasma pulses.

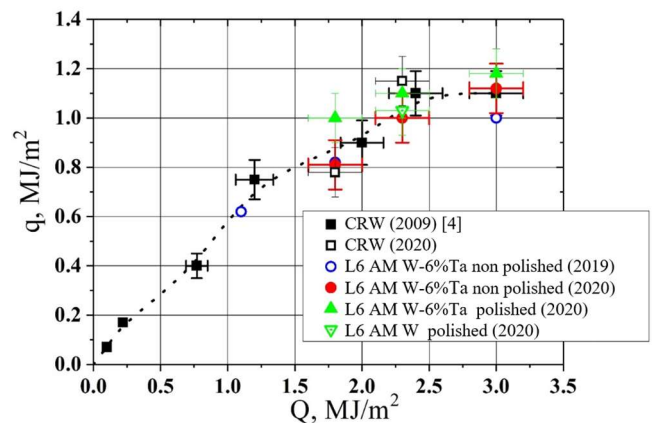


FIG 6 The energy density (q) absorbed by the target surface vs. the energy density (Q) of the impacting plasma stream. Black squares – results for CRW targets [5], other symbols – results of 2019/2020 years.

3.2.2. Plasma surface interaction

During the HHF testing, the PSI is accompanied by particles emitted from the exposed target surfaces (FIG 7 - FIG 9). A large number of ejected particles is observed under plasma impact with energy density causing strong melting/pronounced evaporation. The number of ejected particles is at maximum during the first pulse and decreased with the increasing number of plasma pulses. The overheated

edges of the targets are observed on the camera frames (FIG 7 - FIG 8).

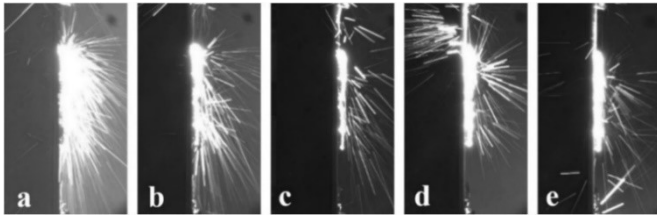


FIG 7 Images of PSI during plasma impact of polished latticed W-6%Ta samples (energy density of incoming plasma $2.3 \text{ MJ}\cdot\text{m}^{-2}$). Images a, b, c, d, e obtained during 1st, 2nd, 3rd, 4th, and 5th plasma pulse respectively.

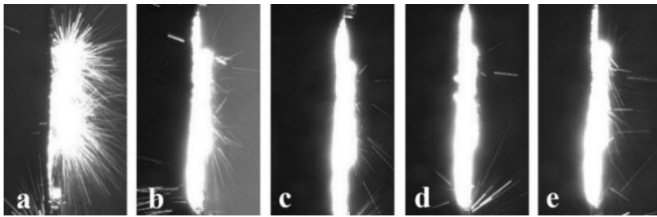


FIG 8 Images of PSI during plasma impact of polished latticed W samples (energy density of incoming plasma $2.3 \text{ MJ}\cdot\text{m}^{-2}$). Images a, b, c, d, e obtained during 1st, 2nd, 3rd, 4th, and 5th plasma pulse respectively.

3.2.3. Polishing effect

The difference between particle ejection from non-polished and polished latticed W-6%Ta samples is negligible. Polished lattices demonstrate a smaller number of separated particles during the first plasma pulses when the sample cleaning occurs. Nevertheless, a large number of ejected particles was registered at a large energy density ($3 \text{ MJ}\cdot\text{m}^{-2}$)

3.2.4. Material effect

The exposure of polished latticed W samples to an applied plasma stream energy of $2.3 \text{ MJ}\cdot\text{m}^{-2}$ FIG 9b caused less particle ejection in comparison with polished AM W-6%Ta (FIG 9a). Almost the absence of ejection is observed during the exposition of the CRW (FIG 9c).

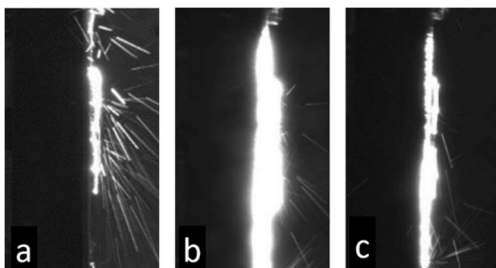


FIG 9. PSI Images during third plasma impact of polished latticed, W-6%Ta (a), W (b) and CRW samples (c) energy density of incoming plasma $2.3 \text{ MJ}\cdot\text{m}^{-2}$.

3.2.5. Sample Mass loss

The results of the mass loss during the experiment (ΔM in mg) are presented in Table 3. The non-uniform mass losses for samples for a given energy density delivered (Q) is due to material outgassing and removal of weakly bounded fragments from the surface specifically for the AM sample. The larger mass loss of the polished AM W sample despite lower particle ejection than AM W-6%Ta is thought to be due to the larger size of debris detached from the sample.

Polishing of the W-6%Ta appears to have a positive effect of reducing the mass loss witnessed during plasma exposure. TABLE 3 AVERAGE ΔM IN mg PER ONE SAMPLE, AFTER 5 PULSES AT GIVEN ENERGY DENSITY EXPOSURE Q

Sample type	1.8 $\text{MJ}\cdot\text{m}^{-2}$	2.3 $\text{MJ}\cdot\text{m}^{-2}$	3 $\text{MJ}\cdot\text{m}^{-2}$
L6 AM W-6%Ta non-polished	9.75	16.85	14.89
L6 AM W-6%Ta polished	5.54	9.51	10.59
L6 AM W polished	Not tested	30.56	Not tested
CRW	1.56	1.63	Not tested

4. CONCLUSIONS

In order to support the development of sacrificial limiters for DEMO, the process parameters for LPB AM production of W-6%Ta lattices were investigated and optimal production conditions were identified.

W-6%Ta, and W lattice samples optimised in a previous study [4], were characterised for geometric accuracy. We concluded that the Fraunhofer samples demonstrate superior geometric conformity and this is presumably because they use a continuous laser. The pulsed technique appears to lead to overbuild which we witnessed in all samples.

The thermal diffusivity of the AM W-6%Ta material is lower when compared to a W plate sample. This is believed to be the result of alloying with Ta, which causes a reduction in thermal conductivity in a similar way to Re alloying with W [7]. Further studies of this are required to understand how microstructural features such as the strong build texture and porosity typically associated with AM materials could also influence this behaviour.

Behaviour of W-6%Ta and W AM lattices under transient plasma loading was compared to CRW. Samples were exposed with up to five 0.25 ms pulses in QSPA Kh-50 with energy density in incoming plasma streams of $1.8 \text{ MJ}\cdot\text{m}^{-2}$, $2.3 \text{ MJ}\cdot\text{m}^{-2}$, or $3 \text{ MJ}\cdot\text{m}^{-2}$, which are respectively above the

expected melting threshold, near and above the expected evaporation threshold [5]. Energy transfer to exposed surfaces was measured during repetitive pulses, the difference in absorbed heat by the different samples at equal plasma energy density was negligible. The PSI observation in this test shows that the number of ejected particles decreases with the number of pulses, and that polishing the plasma-facing surface has a negligible effect on reducing the number of particles ejected for the W-6%Ta sample. Polished W AM samples exhibit a smaller amount of particle ejection than W-6%Ta samples, while CRW samples showed almost an absence of ejection. The mass loss at equal plasma energy exposure was greatest for polished W AM, probably due to the larger size of debris detached from the sample, followed by un-polished W-6%Ta AM, subsequently polished W-6%Ta, and lastly CRW.

It was also observed that under HHF testing, energy absorbed by latticed and CRW targets is similar, suggesting that they may be used for limiter applications and bring the added advantage of adjustment of the heat transfer and stiffness performance by geometry design or material properties. Although AM material has a higher mass loss due to the particle ejection especially in the first PSI event, the impact of this has to be assessed before its suitability for use can be confirmed. The reduced particle ejection after five pulses, however, suggests that this might allow for an AM limiter that can maintain integrity after multiple HHF plasma contact events.

ACKNOWLEDGEMENTS

Thank you to Katja Hunger at IPP (Garching) for the polishing of samples.

This work has been carried out within the framework of the EUROfusion Consortium and has received funding from the Euratom research and training programme 2014-2018 and 2019-2020 under grant agreement No. 633053 and from EPSRC [grant number EP/T012250/1]. The views and opinions expressed herein do not necessarily reflect those of the European Commission.

REFERENCES

- [1] F. Maviglia, R. Albanese, R. Ambrosino, W. Arter, C. Bachmann, T. Barrett, G. Federici, M. Firdaous, J. Gerardin, M. Kovari, V. Loschiavo, M. Mattei, F. Villone, R. Wenninger, "Wall protection strategies for DEMO plasma transients", *Fusion Engineering and Design* Volume 136, Part A, November 2018, Pages 410-414 <https://doi.org/10.1016/j.fusengdes.2018.02.064>
- [2] R. de Luca, P. Fanelli, S. Mingozzi, G. Calabrò, F. Vivio, F. Maviglia and J. You, "Parametric design study of a substrate material for a DEMO sacrificial limiter," *Fusion Engineering and Design*, vol. 158, 2020. <https://doi.org/10.1016/j.fusengdes.2020.111721>
- [3] D. Wang, Z. Wang, J. Ma, K. Li, W. Liu and Z. Shen, "Cracking in laser additively manufactured W: Initiation mechanism and a suppression approach by alloying," *Materials and Design*, vol. 162, pp. 384-393, 2019. <https://doi.org/10.1016/j.matdes.2018.12.010>
- [4] A. v. Müller, G. Schlick, R. Neu, C. Anstätt, T. Klimkait, J. Lee, B. Pasher, M. Schmitt and C. Seidel, "Additive manufacturing of pure tungsten by means of selective laser beam melting with substrate preheating temperatures up to 1000 °C," *Nuclear Materials and Energy*, vol. 19, pp. 184-188, 2019. <https://doi.org/10.1016/j.nme.2019.02.034>
- [5] I.E. Garkusha et al. / Experimental study of plasma energy transfer and material erosion under ELM-like heat loads *Journal of Nuclear Materials* 390–391 (2009) 814–817 <https://doi.org/10.1016/j.jnucmat.2009.01.215>
- [6] M. Fukuda, A. Hasegawa, S. Nogami, Thermal properties of pure tungsten and its alloys for fusion applications, *Fusion Eng. Des.* 132 (2018) 1–6. <https://doi.org/10.1016/j.fusengdes.2018.04.117>.
- [7] Fujitsuka, M., Tsuchiya, B., Mutoh, I., Tanabe, T., & Shikama, T. (2000). Effect of neutron irradiation on thermal diffusivity of tungsten-rhenium alloys. *Journal of Nuclear Materials*, 283–287(PART II), 1148–1151. [https://doi.org/10.1016/S0022-3115\(00\)00170-7](https://doi.org/10.1016/S0022-3115(00)00170-7)
- [8] Savchenko, I. V., & Stankus, S. V. (2008). Thermal conductivity and thermal diffusivity of tantalum in the temperature range from 293 to 1800 K. *Thermophysics and Aeromechanics*, 15(4), 679–682. <https://doi.org/10.1007/s11510-008-0017-z>
- [9] Marinelli, G., Martina, F., Ganguly, S., Williams, S., Lewtas, H., Hancock, D., Mehraban, S., & Lavery, N. (2019). Microstructure and thermal properties of unalloyed tungsten deposited by Wire + Arc Additive Manufacture. *Journal of Nuclear Materials*, 522, 45–53. <https://doi.org/10.1016/j.jnucmat.2019.04.049>
- [10] Oh, G. Y., Kim, Y. K., Kim, S. K., Lim, H. K., & Kim, Y. J. (2017). Effects of grain size and texture on thermal conductivity of AZ31 during static recrystallization. *Materials Transactions*, 58(8), 1241–1243. <https://doi.org/10.2320/matertrans.M2017126>

--